Adsorption of 2-propanol on MgO surface: A combined experimental and theoretical study

Silvia A. Fuente [a],*, Cristián A. Ferretti [b], Nicolás F. Domancich [a], Verónica K. Díez [b], Carlos R. Apesteguía [b], J. Isabel Di Cosimo [b], Ricardo M. Ferullo [c], Norberto J. Castellani [a]

[a] Group of Materials and Catalytic Systems (GMSC) – Department of Physics (UNS-CONICET), Av. Alem 1253, 8000 Bahía Blanca, Argentina
[b] Catalysis Science and Engineering Research Group (GICIC) – INCAPE (UNL-CONICET), Santiago del Estero 2654, 3000 Santa Fe, Argentina
[c] INQUISUR, Department of Chemistry (UNS), Av. Alem 1253, 8000 Bahía Blanca, Argentina

ABSTRACT

The adsorption of 2-propanol (or isopropanol) on MgO was studied using infrared (IR) spectroscopy and density functional theory (DFT) simulations. The analysis of IR spectra indicates that the molecule can adsorb either molecularly or dissociatively. DFT calculations show that the adsorption mode depends on the active site of the catalyst. While on perfect terrace it adsorbs non-dissociatively, on edge and on threefold coordinated O anion (O-corner sites) the adsorption occurs dissociatively by breaking the O—H bond without activation barrier giving 2-propoxide and a surface hydroxyl group. Calculations also suggest that vacant oxygen centers on terrace, edge and corner are also possible sites for non-dissociative adsorption. On Mg ions located at corners the adsorption is strong but non-dissociative, while on a Mg vacancy at the same position the molecule easily dissociates. Frequency modes are also calculated and compared in detail with experimental IR spectra.

© 2014 Elsevier B.V. All rights reserved.

1. Introduction

The production of fungible fuels from biomass offers a possible contribution to meet growing energy demands and to reduce their environmental impact. The pyrolysis of biomass produces liquid oil (Bio-oil) constituted mostly by oxygenated compounds, which are of great interest as fuel and fine chemicals. Studies have been conducted to improve the quality of Bio-oil as fuel and chemicals through catalytic processes with inorganic acid solids [1–3]. Gayubo et al. [4] studied the catalytic transformation of several model components of biomass pyrolysis oil, such as phenols and alcohols as 1-propanol, 2-propanol, 2-butanol, with HZSM5 zeolite obtaining mainly light olefins and aromatic compounds. The alcohol decomposition, used in these catalytic processes, is also performed as a test for evaluating the catalytic acid–base properties of such as metal oxides. Alcohol dehydrogenation products, aldehydes and ketones, are preferentially formed on basic catalysts, while the formation of dehydration products, olefins and ethers, is favored by acid catalysts [5]. The 2-propanol decomposition over basic sites occurs through an elimination reaction yielding acetone, whereas over acid sites, 2-propanol dehydrates to propylene and to diisopropyl ether [6].

The MgO is a base solid used in several important chemical applications, particularly in heterogeneous catalysis. Its surface presents strongly electron-donating oxygen ions and moderate electron-accepting magnesium cations making this catalyst appropriate for several reactions, such as the dehydrogenation of alcohols [6], the hydrogenation of unsaturated ketones by hydrogen transfer reduction [7], the aldol condensation [8], the Cannizzaro and Tischenko reactions [9], the Michael, Witting and Knoevenagel reactions [10] and the transesterification of alkyl esters [11].

In the most stable crystallographic plane of MgO, i.e. (1 0 0), there are many surface irregularities resulting from different types of exposed Mg—O pairs. The Mg^{2+} and O^{2-} ions have different coordination numbers depending on their location on terraces, edges and corners with five-, four- and threefold coordination, respectively. They are commonly denoted as Mg^{2+}_{LC} or O^{2-}_{LC} (LC means for coordination number). Among the possible point defect sites, the most studied has been the F_s one, generated by the removal of a neutral O atom from the MgO surface; consequently, two electrons are trapped inside the produced cavity. Mg vacancies, known as V_s centers, are generated by the extraction of a neutral surface
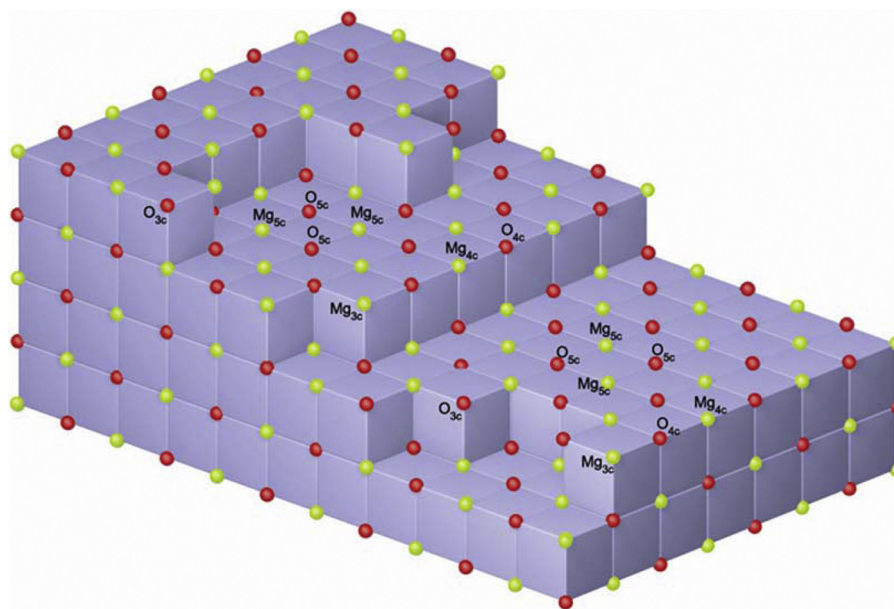
Fig. 1. Schematic representation of irregularities on the MgO (1 0 0) surface, with O_{LC} and Mg_{LC} ions in different positions.

Mg atom, causing a positively charged cavity. A schematic representation of the MgO surface without punctual F_s and V_s defects is presented in Fig. 1.

In order to study the acid–base properties of MgO surfaces, several theoretical and experimental procedures have been employed, particularly appealing to adsorption tests [12–14]. Theoretical studies have revealed that molecules such as methanol or water do no dissociate on terrace sites of MgO (1 0 0), with and without defects. In particular, the capacity to produce a proton abstraction is, in general, associated with the value of L; the ions with lower coordination numbers ($L = 3$) being more reactive that those with higher ones ($L = 5$) [15–18].

In the present work the adsorption of 2-propanol (or isopropanol, IPA) on MgO (1 0 0) is experimentally and theoretically studied. The experimental approach comprises the determination of infrared (IR) spectra for the IPA/MgO system. On the other hand, we have considered the adsorption of an IPA molecule on different terrace, edge and corners sites of MgO with cluster models within the framework of DFT. We are interested in making a comparison between both IR spectroscopy and theoretical results, in order to analyze how the adsorption capacity of the active site is related with its local electronic structure.

2. Experimental

2.1. Catalyst synthesis

Magnesium oxide was prepared by hydration of commercial MgO (Carlo Erba, 99%). 250 ml of distilled water were slowly added to 25 g of commercial MgO and stirred at room temperature. The temperature was then raised to 353 K and stirring was maintained for 4 h. Excess of water was removed by drying the sample in an oven at 358 K overnight. The resulting $Mg(OH)_2$ was decomposed in N_2 (30 ml/min) to obtain MgO which was then treated for 18 h in N_2 at 773 K.

BET surface areas were determined by N_2 physisorption at 77 K in a NOVA-1000 Quantachrom sorptometer and the structural properties of MgO catalysts were analyzed by X-ray diffraction (XRD) using a Shimadzu XD-D1 diffractometer equipped with Cu-$K\alpha$ radiation source ($\lambda = 0.1542$ nm).

Catalyst basic properties were measured by temperature programmed desorption (TPD) of CO_2. For the TPD experiment, the sample was pretreated in situ in a N_2 flow at 773 K to remove water and carbonates formed during storage, cooled down to room temperature, and then exposed to a flowing mixture of 3% of CO_2 in N_2 until surface saturation was achieved (5 min). Weakly adsorbed CO_2 was removed by flushing with N_2. Finally, the temperature was increased to 773 K at a ramp rate of 10 K/min. Desorbed CO_2 was converted in CH_4 on a methanation catalyst (Ni/Kieselghur), and then analyzed using a flame ionization detector (FID). Total base site numbers (N_b, μmol/g) were measured as the evolved CO_2 obtained by integration of TPD curves.

2.2. Infrared (IR) spectra characterizing MgO samples

Experiments were carried out using an inverted T-shaped cell containing the sample pellet and fitted with CaF_2 windows. Data were collected in a Shimadzu FTIR Pestige-21 spectrometer. The absorbance scales were normalized to 20 mg pellets. The sample was pretreated in vacuum at its corresponding stabilization temperature and cooled to room temperature; later on, the spectrum of the pretreated catalyst was obtained. After admission of 2-propanol ($P_{iIPA} = 32$ Torr) to the cell at room temperature, spectra were taken sequentially at increasing adsorption times for 15 min. The sample was then evacuated for 15 min at room temperature and the resulting spectrum was recorded. Spectra of the adsorbed species were obtained by subtracting the catalyst spectrum.

2.3. Computational details

Density functional theory (DFT) molecular orbital calculations were carried out using the gradient corrected Becke's three parameters hybrid exchange functional in combination with the correlation functional of Lee, Yang and Parr (B3LYP) [19]. This method was widely used in the past to study adsorption processes yielding reliable results on oxides clusters.

The terrace site at MgO (1 0 0) surface was represented by the cluster indicated as $Mg_{25}O_{25}(Mg\text{-}ECP)_{25}$ consisting of two layers (first layer: Mg_9O_{16}; second layer: $Mg_{16}O_9$). To take into account the Madelung field due to the rest of the extended oxide, the cluster was embedded with an array of ±2 point charges. Moreover, the
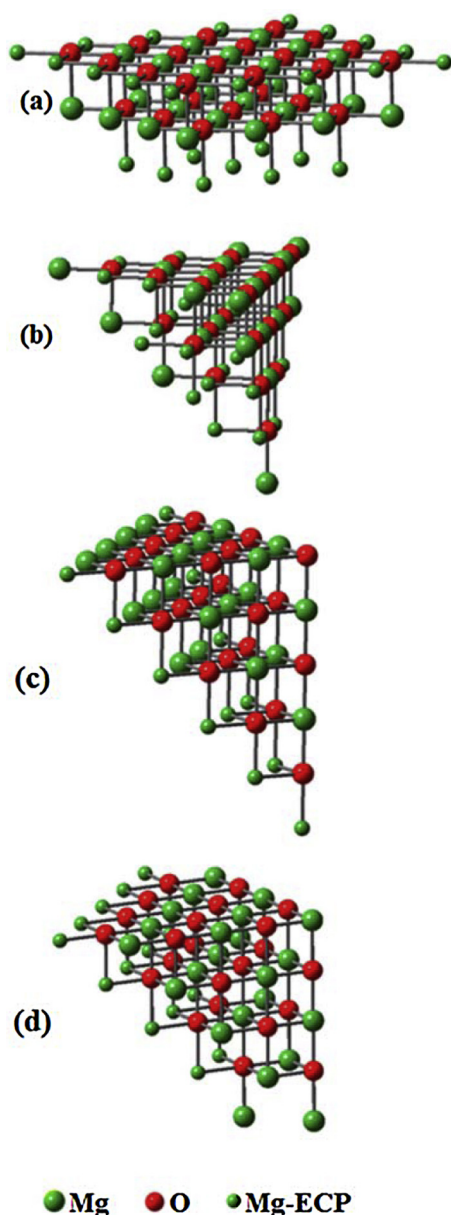
Fig. 2. Cluster used in this work for modeling MgO surface: (a) perfect terrace site, $Mg_{25}O_{25}$ (Mg-ECP)$_{25}$; (b) edge site, $Mg_{22}O_{22}$(Mg-ECP)$_{19}$; (c) O-corner site, $Mg_{22}O_{22}$(Mg-ECP)$_{12}$ and (d) Mg-corner site, $Mg_{23}O_{23}$(Mg-ECP)$_{14}$.

positive point charges at the interface were replaced by effective core potentials (ECP) corresponding to Mg^{2+} to account for the finite size of the cations and to avoid spurious charge polarization. The corresponding $Mg_{25}O_{25}$(Mg-ECP)$_{25}$ cluster is represented in Fig. 2a. This embedding technique was used previously for the study of both bulk and surface properties giving results which are in good agreement with those obtained by periodic calculations [20–23].

On a perfect MgO (1 0 0) surface, Mg^{2+} and O^{2-} ions are five-fold coordinated (Mg_{5c} and O_{5c}). However, since the MgO catalyst used in our IR experiments has a high-surface area, models representing surface ions with lower coordination numbers (L) are needed. To take into account this fact, we carried out a molecular modeling of the IPA/MgO system using four cluster models representing four different adsorption sites of the real MgO surface, as depicted in Fig. 1: terrace sites containing the Mg_{5c}–O_{5c} pairs ($L = 5$); edge and O-corner sites corresponding to O_{4c} ($L = 4$) and O_{3c} ($L = 3$), respectively; and Mg-corner centers (Mg_{3c}; $L = 3$).

The $Mg_{22}O_{22}$(Mg-ECP)$_{19}$ cluster was used to represent an edge defect, obtained by the intersection of two [1 0 0] and [0 1 0] oriented planes. O-corner and Mg-corner sites were represented by the $Mg_{22}O_{22}$(ECP)$_{12}$ and $Mg_{23}O_{23}$(Mg-ECP)$_{14}$ clusters, respectively, both due to the intersection of the three [1 0 0], [0 1 0] and [0 0 1] oriented planes. These clusters are shown in Fig. 2b–d, respectively).

While the atomic orbitals of the oxygen ion acting as the adsorption site and its nearest exposed O neighbors (four for terrace and edge sites, or three for corner site) were described by the 6–31++G** basis set, those of the exposed Mg ions directly bonded with the O adsorption site (also four for terrace and edge sites and three for corner site) were expressed using the 6–31G** basis set; for the rest of Mg and O ions of the cluster, the 6–31G basis set was considered. The atoms belonging to the IPA molecule are expanded by the 6–31G** basis set.

For terrace, edge and O-corner clusters, a neutral F_s center was represented by eliminating an O atom from the clusters mentioned above. In these cases, the geometrical optimization included the nearest exposed Mg atoms surrounding the vacancy (four for terrace and edge and three for corner site). On the cluster representing the Mg ion at corner, a V_s site was modeled by eliminating a neutral Mg atom, and the geometrical optimization included the three O exposed atoms surrounding the vacancy. While F_s are electron donor centers, V_s sites show a strong tendency to capture electronic charge. Only the V_s defect at corner position was considered.

For the calculation of the optimized adsorbed structures, as starting geometry the IPA molecule was always placed close to the corresponding active site in its molecular form (i.e., non-dissociated). As we shall see later, in several cases the O—H bond breaks spontaneously without activation barrier.

The adsorption energy E_{ads} was evaluated according to the following total energies difference:

$$E_{ads} = E_{IPA/MgO\ cluster} - E_{MgO\ cluster} - E_{IPA} \qquad (1)$$

The adsorption energies calculated in this way present an error known as base set superposition error (BSSE), which is usually corrected using the counterpoise procedure (CP) by means of ghost orbitals [24]. Here, we have used an alternative methodology to minimize such an error and then to estimate its magnitude. For that, single point calculations were performed for several physisorbed and chemisorbed modes using the more extended 6–311++G (3df, 2p) basis set which is known to reduce the BSSE considerably [25]. For all the cases studied, adsorption energies resulted to be about 0.10 eV less stable than those calculated using Eq. (1). Therefore, according to these results, BSSE correction does not seem to modify the general trends obtained from the uncorrected adsorption energies.

Atomic net charges were calculated following the natural bond orbital (NBO) scheme [26], which gives realistic values for the charge partitioning. For the later analysis of vibrational frequency spectra of adsorbed IPA a careful study for free and adsorbed molecules was performed. The calculated frequencies have been scaled with a factor of 0.96 [27].

All the calculations have been performed using the Gaussian-03 program package [28].

3. Results and discussion

3.1. Characterization of MgO

The hydration of commercial MgO and subsequent decomposition and stabilization at 773 K, the BET surface increased from 27 to 189 m²/g due to the development of a porous structure because of gaseous evolution during Mg(OH)$_2$ decomposition [29]. MgO had a pore volume of 0.38 ml/g and a mean pore diameter of about 80 Å.
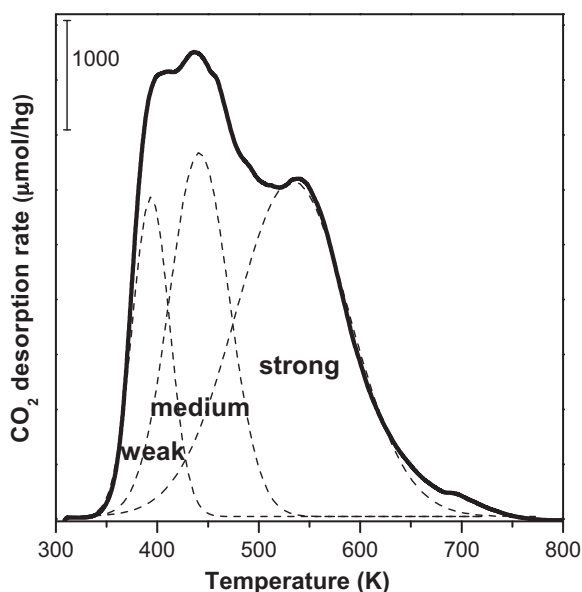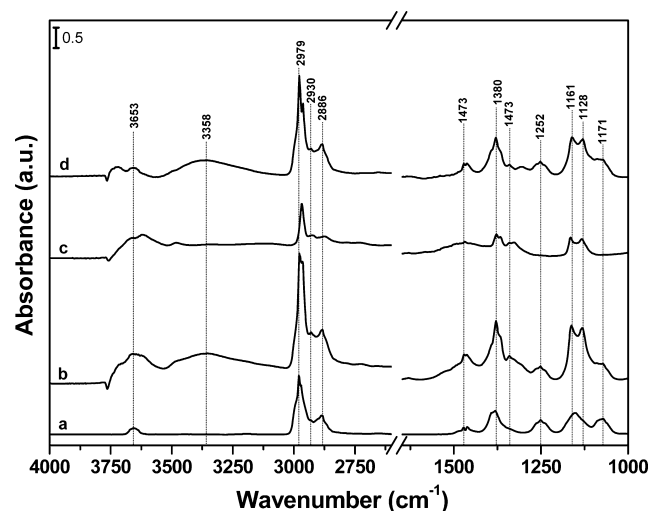
Fig. 3. TPD profile of CO_2 on MgO.

Fig. 4. FTIR spectra of species resulting at room temperature of: (a) 32 Torr 2-propanol vapor phase; (b) 32 Torr 2-propanol on MgO; (c) followed by evacuation and (d) difference of spectra (b) and (c).

Table 1
Observed and calculated frequencies (cm^{-1}) for gas phase 2-propanol.

Assignments	Experimental	Calculated
$\nu(O{-}H)$	3653	3643
$\nu(C{-}H_3)_a$	2979, 2971	3007, 3005
$\nu(C{-}H_3)_s$	2930	2984
$\nu(C{-}H)$	2884	2933
$2\delta(C{-}H_3)_a$	–	–
$\delta(C{-}H_3)_a$	1472, 1461	1459, 1451
$\delta(C{-}H_3)_s$	1391, 1381	1374, 1365
$\gamma(C{-}H)$	1340	1314
$\delta(C{-}H), \delta(O{-}H)$	1262, 1251, 1239	1264
$\nu(C{-}C), \rho(C{-}H_3)$	1153	1145
	1130	1104
$\nu(C{-}C), \rho(C{-}H_3)$	1074	1047

X-ray diffractogram of catalyst (not shown here) did only a single phase of MgO periclase (ASTM 4-0829).

The surface base properties of the MgO were investigated by TPD measurement the CO_2 preadsorbed at room temperature. The CO_2 desorption rate as a function of sample temperature is shown in Fig. 3. The total base site number, N_b (μmol/g), calculated by integration of TPD profile as the total amount of CO_2 desorbed from the catalyst, was 655 μmol/g.

In previous work [30] we used FTIR preadsorbed at room temperature to study the chemical nature of surface oxygen species on similar high-surface area MgO catalyst. By this technique, several CO_2 adsorbed species formed on different oxygen-containing species or on oxygen anions with different coordination number could be detected. We identified at least three different CO_2 adsorption species: unidental carbonate (U.C.) formation requires isolated surface O^{2-} ions, i.e., coordinatively unsaturated anions, such as those present in corners or edges (O_{3c} or O_{4c}) and exhibits a symmetric O—C—O stretching at 1360–1400 cm^{-1} and an asymmetric O—C—O stretching at 1510–1560 cm^{-1}. Bidentate carbonate (B.C.) form on Lewis acid–Brønsted base pairs such as $Mg_{5c}{-}O_{5c}$ pairs predominant on the terrace sites of MgO and show a symmetric O—C—O stretching at 1320–1340 cm^{-1} and an asymmetric O—C—O stretching at 1610–650 cm^{-1}. Bicarbonate (Bic) species formation involves surface hydroxyl groups and shows a C—OH bending mode at 1220 cm^{-1} as well as symmetric and asymmetric O—C—O stretching bands at 1480 cm^{-1} and 1650 cm^{-1}, respectively [31,32].

The FTIR analysis of CO_2 adsorbed at room temperature and evacuation at 298, 373, 473 and 573 K was carried out on MgO sample, confirmed the formation of different carbonate species on a heterogeneous MgO surface, and shows that the Bic species disappeared after evacuation at 373 K revealing the weak basicity of surface OH^- groups on MgO. In contrast, U.C. and B.C. species remained on the surface even after evacuation at 573 K, although the U.C. species were more resistant to evacuation at higher temperatures. Thus, results suggested the following base strength order for the surface oxygen species on MgO: low coordination O^{2-} anions > oxygen in $Mg^{2+}{-}O^{2-}$ pairs > OH^- groups.

Based on the FTIR results, the TPD profile of Fig. 3 was deconvoluted in three desorption bands, reaching maximum desorption rates about 400, 450, and 550 K. Although CO_2 desorption follows first-order kinetics, for simplicity we have used Gaussian functions

for the deconvolution and integration of the TPD traces. The base site densities in μmol/m^2, either total or the contribution of each basic species, were calculated then from the integration areas of the TPD profile after correcting by the surface area and assuming a CO_2:surface base site = 1:1 desorption stoichiometry. The total base site density (n_b) was 3.47 μmol/m^2 and the contribution of each band, identified as the density of weak (n_{OH}), medium (n_{Mg-O}) and strong (n_O) base sites, were 0.55 μmol/m^2, 1.26 μmol/m^2 and 1.66 μmol/m^2, respectively.

3.2. Infrared study of adsorption of 2-propanol on MgO at room temperature

The infrared spectrum of the 30 Torr 2-propanol gas phase expanded into the IR cell at room temperature (Fig. 4a) shows only diagnostic absorption bands of free 2-propanol molecules [33–35]. The band at 3653 cm^{-1} is due to OH stretching modes ($\nu(O{-}H)$), whereas the band at 1251 cm^{-1} is mainly due to OH bending mode ($\delta(O{-}H)$). The peaks around 2900 cm^{-1} are assigned to the C—H_3 and C—H stretching modes ($\nu(C{-}H_3)$ and $\nu(C{-}H)$), whereas the peaks within the 1500–1200 cm^{-1} interval are due to C—H_3 and C—H bending ($\delta(C{-}H_3)$ and $\delta(C{-}H)$). Other observed bands are: C—O stretching ($\nu(C{-}O)$, 1100–1000 cm^{-1}), C—H wagging ($\gamma(C{-}H) \approx 1300\ cm^{-1}$), C—C stretching ($\nu(C{-}C) \approx 1100\ cm^{-1}$) and C—$H_3$ rocking ($\rho(C{-}H_3)$, 1100–1000 cm^{-1}). The detailed assignments of the IPA FTIR spectrum are given in Table 1.

The spectrum of MgO evacuated at 773 K (not shown) displays an asymmetric peak at about 3755 cm^{-1}, with a shoulder on the

Table 2
Assignments of vibration modes for non-dissociative 2-propanol on MgO experimental and obtained by DFT calculation.

Assignments	Experimental	Calculated				
		Terrace	Mg-corner	F_s-terrace	F_s-edge	F_s-corner
ν(O—H)	3723, 3656, 3325	3124	2889	3129	2981	3039
ν(C—H$_3$)$_a$	2979, 2962	2999, 2987	3002, 2998	3005, 3003	3009, 3004	3010, 3008
ν(C—H$_3$)$_s$	2930	2975	2989	2984	2986	2993
ν(C—H)	2886	2914	2945	2915	2918	2948
2δ(C—H$_3$)$_a$	–	–	–	–	–	–
δ(C—H$_3$)$_a$	1473, 1463	1462, 1454	1457, 1450	1459, 1442	1458, 1445	1457, 1445
δ(C—H$_3$)$_s$	1393, 1380	1437, 1433	1436, 1434	1439, 1430	1437, 1433	1437, 1433
γ(C—H)	1340	1394	1377	1351	1360	1361
δ(C—H), δ(O—H)	1261, 1252, 1241	1310	1308	1314	1317	1332
ν(C—C), ρ(C—H$_3$)	1161	1144	1145	1142	1137	1138
	1128	1112	1112	1108	1114	1115
ν(C—C), ρ(C—H$_3$)	1071	1083	1106	1069	1077	1074

[a] ν(O$_s$—H).

lower frequency side, attributed to isolated OH groups on kinks and edges, and a broad band centered at 1500 cm^{-1}, assigned to residual carbonates [36,37].

2-Propanol was admitted at room temperature in the IR cell containing a 20 mg wafer of MgO, previously degassed at 773 K, and spectra were then taken during adsorption at intervals of 2.5 min during 15 min. After 10 min, the spectra did not show changes in the signal intensity (Fig. 4b). The bands remaining on MgO after the 2-propanol adsorption at room temperature does not differ very much from those of IPA gas. The bands at 3710, 3653, 1630 cm^{-1}, and the shoulder corresponding to the bands between 3530 and 3130 cm^{-1} suggest the presence hydrogen-bonded IPA interacting with initially present surface hydroxyl groups and with adsorbed water [38]. The ν(O—H) bands as well as the δ(O—H) band at 1251 cm^{-1} observed in the IR spectrum indicate that a particular form of non-dissociated 2-propanol was adsorbed on MgO. The bands at 2979, 2930 and 2886 cm^{-1} assigned to ν(C—H$_3$)$_a$, ν(C—H$_3$)$_s$ and ν(C—H) vibrations also appear together with bands at 1469, 1367, 1340, 1164 and 1133 cm^{-1}, characteristic of surface 2-propoxide species bonded to Mg^{2+} sites [39–41]. These results indicate the presence of two types of alcohol-derived surface species upon adsorption of 2-propanol on MgO: (a) molecularly adsorbed 2-propanol and (b) 2-propoxide species bonded to surface Mg^{2+} cations. The main experimental frequencies are summarized in Tables 2 and 3 for non-dissociative and dissociative adsorptions, respectively.

After the 2-propanol excess evacuation at room temperature, the resulting spectrum is displayed in Fig. 4c. Evacuation at room temperature caused the reduction of the band intensity at 3750–3600 cm^{-1} and the disappearance of the shoulder corresponding to the bands between 3530 and 3130 cm^{-1}, indicating

that a non-dissociated form of IPA was mainly desorbed in these conditions. The ν(O—H) band at 3483 cm^{-1} is a clear indicative of chemisorbed 2-propanol [42]. After such treatment, the spectrum of the adsorbed species showed bands corresponding to 2-propoxide species coordinated to Mg^{2+} sites (Lewis acid). The principal bands at 2967, 2926, 2897 and 2876 cm^{-1} assigned to ν(C—H$_3$)$_a$, ν(C—H$_3$)$_s$, 2δ(C—H$_3$)$_a$ and ν(C—H) vibrations, together with bands at 1469, 1377, 1367, 1168 and 1133 cm^{-1} characteristic of δ(C—H$_3$)$_a$, δ(C—H$_3$)$_s$, ν(C—C), ν(C—O) and ρ(C—H$_3$) modes, respectively, indicate the formation of isopropoxide species through dissociative adsorption of 2-propanol [39,43]. The disappearance of the strongest δ(C—H), δ(O—H) bands about 1260–1240 cm^{-1} indicates that the isopropoxide groups are the adsorbed species mostly present on the catalyst surface [44]. The frequencies and assignments of these species are summarized in Table 2. Similar assignments were obtained with related metal oxides such as γ-Al$_2$O$_3$ [45], TiO$_2$ [46], ZrO$_2$ [47], and UO$_2$ [48].

The spectrum of Fig. 4d was obtained by subtracting the spectrum resulting from admission at room temperature of IPA on MgO (Fig. 4b) from the one resulting from evacuation at room temperature (Fig. 4c). All the remaining bands in the IR spectrum obtained under these conditions may be assigned to physisorbed 2-propanol, confirming that such species are desorbed by evacuation at room temperature [33–36]. The observed frequencies are also summarized in Table 3.

3.3. Theoretical study of adsorption of 2-propanol on MgO

In Fig. 5, the optimized structures corresponding to the 2-propanol conformers are shown. This molecule presents three conformers [49]. Two of them (gauche conformations) are

Table 3
Assignments of vibration modes for dissociative 2-propanol on MgO experimental and obtained by DFT calculation.

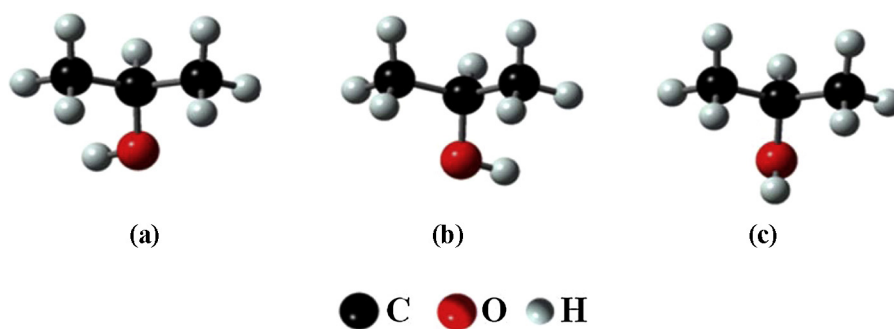| Assignments	Experimental	Calculated		
		Edge	O-corner	V_s-corner
ν(O—H)	3483	2482[a]	3308[a]	3719[a]
ν(C—H$_3$)$_a$	2967	2991, 2977	2974, 2965	3009, 2987
ν(C—H$_3$)$_s$	2926	2969	2952	2955
ν(C—H)	2876	2810	2752	2844
2δ(C—H$_3$)$_a$	2897	2905	2986, 2877	2935, 2880
δ(C—H$_3$)$_a$	1469, 1453	1453	1459	1479
δ(C—H$_3$)$_s$	1377, 1367	1352, 1339	1355, 1340	1379, 1360
γ(C—H)	1340	1301	1313	1305
δ(C—H), δ(O—H)	–	–	–	–
ν(C—C), ρ(C—H$_3$)	1164	1151	1158	1127
	1133	1095	1096	1093
ν(C—C), ρ(C—H$_3$)	1168	983	987	941

[a] ν(O$_s$—H).

Fig. 5. Different optimized geometries of 2-propanol molecule.

equivalent and only differ in their H—C—O—H torsional angles of near 60° and −60°, respectively (Fig. 5a and b). The third conformer (transconformation) corresponds to an H—C—O—H torsional angle of near 180° (Fig. 5c). The two gauche conformations form an enantiomeric pair, and they are rapidly interconverted by quantum-mechanical tunneling constituting a transient chirality system [50]. From the geometrical optimization of all these conformers, the following intramolecular interatomic distances (d) were obtained: $d_{(C–C)} \approx 1.53\,\text{Å}$, $d_{(C–H)} \approx 1.10\,\text{Å}$, $d_{(C–O)} \approx 1.44\,\text{Å}$ and $d_{(O–H)} \approx 0.96\,\text{Å}$. All conformers presented an intramolecular hydrogen bond that plays an important role in the molecular stability. Calculations indicate that conformer (Fig. 5c) is only slightly more stable than (Fig. 5a) and (Fig. 5b).

Optimized geometrical structures for 2-propanol adsorption on a terrace site and on defective (edge and corner) sites of the MgO surface are shown in Fig. 6. The corresponding results for adsorption energies (E_{ads}), intramolecular bond distances (O—H and C—O), and the closest IPA-surface distances to surface atoms (H—O_s and O—Mg_s) are summarized in Table 4.

When IPA is adsorbed on the surface without defects (Fig. 6a), two bonds link the IPA molecule with the MgO surface: a hydrogen bond of 1.760 Å between the alcoholic H atom and a surface oxygen ion (O_s), and a weaker bond of 2.994 Å between the alcoholic O atom and a magnesium ion of the surface (Mg_s). In this non-dissociative adsorption, the IPA O—H bond undergoes a stretching of 0.034 Å, while the C—O bond undergoes a slight shortening of 0.017 Å, compared with the values for the isolated 2-propanol. These geometrical results were similar to those found in previous studies on other alcohols, such as methanol and ethanol on terrace sites of MgO [14,15]. Moreover, the E_{ads} value for IPA adsorbed on the terrace site, about −0.6 eV, is similar to the results obtained previously for alcohol molecules adsorbed on MgO (1 0 0) [14,15].

On the other hand, when IPA is adsorbed on a defective edge site, a dissociative adsorption takes place as a result of a stronger IPA-edge interaction (Fig. 6c). The magnitude of E_{ads} is higher than the one obtained for terrace, by about 0.8 eV, and the $d_{(O–H)}$ distance is longer than the distance at free IPA molecule due to O—H bond breaking, which cause the formation of both a new surface OH between the abstracted H and a surface O_s anion, and a surface isopropoxide species on a surface Mg_s cation. Thus, the $d_{(O–Mg_s)}$ and $d_{(H–O_s)}$ distances were considerably shortened in comparison with the terrace surface structure. The differences between the $d_{(O–Mg_s)}$ and $d_{(H–O_s)}$ distances on edge, in relation to the same distance on terrace, are of 0.93 Å and 0.72 Å respectively.

The adsorption of 2-propanol on the O-corner site is dissociative (Fig. 6e), with an E_{ads} magnitude higher, by about 0.8 eV, than that obtained for edge site, evidencing an even stronger interaction between the IPA at corner in comparison with the regular terrace site. As in the case of the defective edge site, such interaction generates a surface hydroxyl. While the $d_{(O–Mg_s)}$ distance obtained on O-corner was similar to the one at the edge site, the $d_{(H–O_s)}$

distance is shorter by 0.04 Å at the corner. Moreover, O—H and C—O bonds undergo a stretching of 0.80 Å and 0.05 Å, respectively, from the values presented at the isolated molecule.

Noticeably, when 2-propanol is adsorbed on the other defective corner site, i.e., the Mg-corner site (Fig. 6g), the magnitude of E_{ads} value is only 0.2 eV lower than that obtained for the adsorption of IPA on O-corner. Nevertheless, the IPA molecule adsorbed on the Mg-corner site shows a non-dissociative adsorption, which makes the hydroxyl group to maintain its integrity. The $d_{(O–H)}$, $d_{(C–O)}$, and $d_{(H–O_s)}$ distances are similar to those found in terrace, although the $d_{(O–Mg_s)}$ distance was 0.95 Å smaller than that obtained on terrace. In fact, the increase of the surface Mg unsaturation from the terrace to the corner site cause a strong interaction between these atoms, presenting a distance whose value is close to the Mg—O experimental distance (2.106 Å [51]).

In order to attain a more comprehensive view of the IPA–MgO interaction, the adsorption energy was considered as the contribution of two terms:

$$E_{ads} = E_{def} + E^{*}_{ads} \tag{2}$$

where E_{def} is the energy required to distort the geometry from the free molecule to acquire the structure of the adsorbed state, and E^{*}_{ads} is the energy associated with the stabilization of the distorted IPA molecule in the adsorption process. In this way the large distortion due to the dissociation processes can be put more clearly in evidence in terms of these components of the adsorption energy, in such a way that dissociative adsorptions present larger values of E^{*}_{ads} (in magnitude). Notice for example that the E_{ads} values are similar on O-corner (dissociative adsorption) and on Mg-corner (non-dissociative adsorption); however, the corresponding E^{*}_{ads} value is near 4.6 eV more stable for dissociated IPA. Besides, on edge and O-corner (on which the adsorption is dissociative), E^{*}_{ads} value is 2.2 eV larger on O-corner because on this site the identity of the isopropoxide fragment is more clearly defined (Fig. 6c and e).

The most relevant atomic NBO charges for 2-propanol adsorption with respect to the free molecule and pure MgO surface, are summarized in Table 4. The most important modifications observed correspond to the O atoms. In all the sites of smaller coordination number ($L = 3$ and 4), the O atom of alcohol receives negative charge, while surface O_s anions lose electronic charge. These results are in agreement with the strong basic character of the MgO surface. Notice however that, for the sites of smaller coordination, we can observe that both the O atom of IPA and the surface Mg ion receive negative charge from the surface O ion and the H atom of IPA. The transfer to the O atom of IPA is greater for the dissociative adsorptions on edge and O-corner than for the non-dissociative cases on terrace and Mg-corner.

As it was pointed out above, from Table 4 we can infer that the magnitude of E_{ads} is an increasing function of the coordination number (L) of the oxygen ion acting as adsorption site. Indeed,
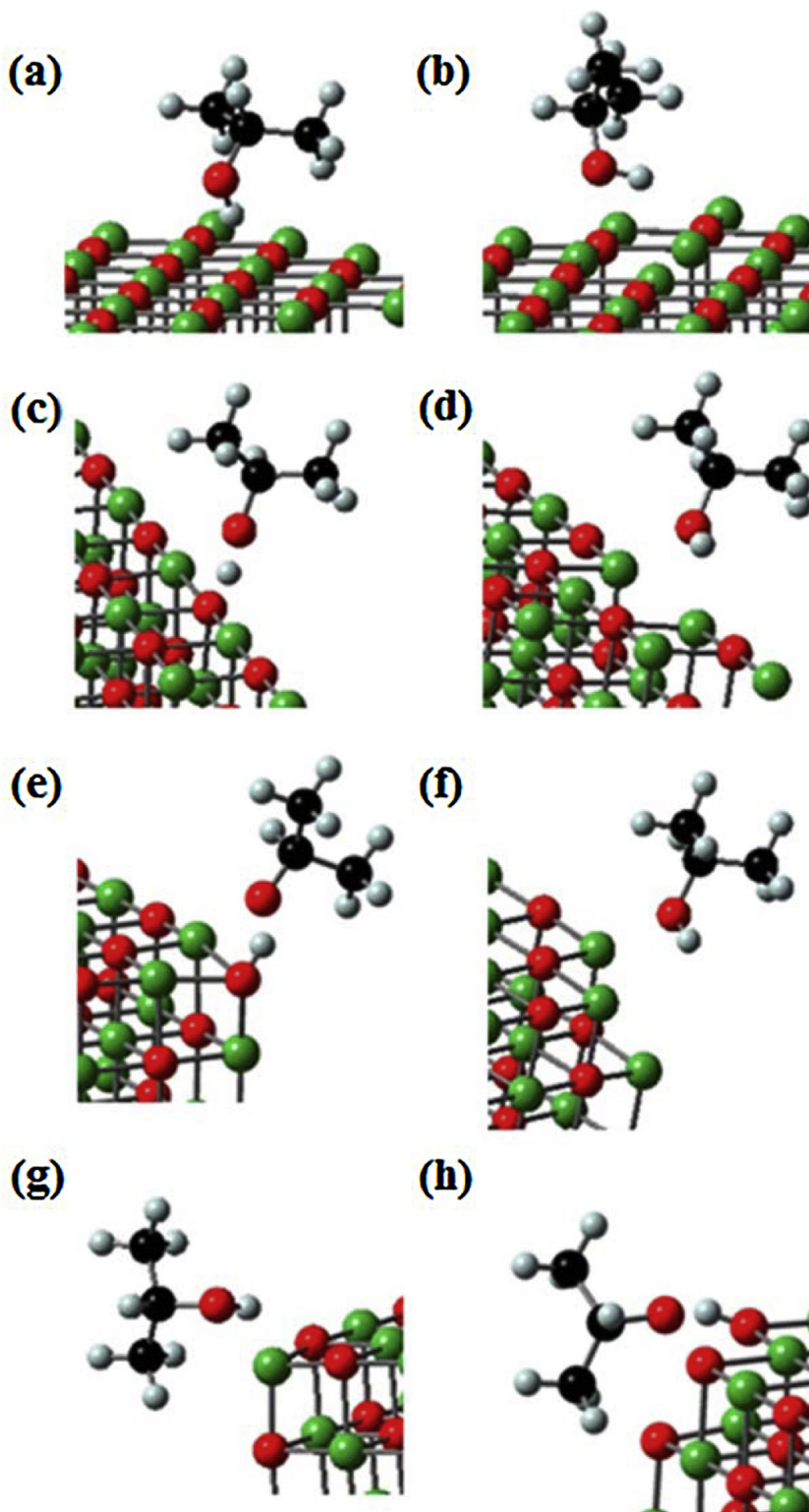
Fig. 6. Optimized geometrical structures of IPA adsorbed on different MgO surface sites. (a) Terrace site; (b) F_s-terrace site; (c) edge site; (d) F_s-edge site; (e) O-corner site; (f) F_s-corner site; (g) Mg-corner site and (h) V_s-corner site.

it changes by a nearly factor of 3.5 from $L = 5$ to $L = 3$. On the other hand, this interaction can be related to the redistribution of atomic charges. In order to show this correlation, in Fig. 7 the values of E^*_{ads} are plotted as a function of the NBO atomic charges for the O atom of IPA. We notice that both quantities are well correlated, including the cases of dissociative adsorption. This means that as the degree of dissociation increases, the negative charge of O belonging to IPA

increases, which in turns is a clear indication of the electrostatic nature of the adsorbate–substrate interaction.

The optimized geometrical structures obtained in the evaluation of IPA adsorption on vacancies, namely, F_s-terrace, F_s-edge, F_s-corner, and V_s-corner are shown in Fig. 6 (b, d, f, h, respectively), and the main molecular properties are summarized in Table 4.

Table 4
Adsorption energies, bond distances (d) and variation of atomic charge (Δq) for IPA adsorption on terrace and different topological defects and vacancies on MgO.

	Regular sites				Vacancies			
	Terrace	Edge	O-corner	Mg-corner	F_s-terrace	F_s-edge	F_s-corner	V_s-corner
E_{ads} (eV)	−0.59	−1.42	−2.16	−1.95	−0.49	−0.93	−0.85	−3.79
E^*_{ads} (eV)	−0.63	−4.48	−6.64	−2.05	−0.54	−1.02	−0.93	−10.30
E_{def} (eV)	0.04	3.06	4.48	0.10	0.05	0.09	0.08	6.51
$d_{(H-O_s)}$ (Å)	1.760	1.031	0.986	1.734	3.217	4.090	3.617	0.965
$d_{(O-Mg_s)}$ (Å)	2.994	1.940	1.920	2.048	2.283	2.050	2.061	2.899
$d_{(O-H)}$ (Å)	0.994	1.481	1.756	1.013	0.994	1.003	0.999	2.638
$d_{(C-O)}$ (Å)	1.423	1.398	1.393	1.450	1.433	1.447	1.449	1.441
$\Delta q(O)$[a]	−0.030	−0.216	−0.235	−0.107	−0.053	−0.123	−0.119	0.464
$\Delta q(H)$[b]	0.048	0.070	0.065	0.083	0.039	0.033	0.042	0.082
$\Delta q(O_s)$	−0.018	0.086	0.292	0.032	−0.008	0.001	0.008	−0.130
$\Delta q(Mg_s)$	−0.015	−0.064	−0.274	−0.128	−0.005	0.148	0.214	−0.001

O_s and Mg_s are the closest surface atoms to the adsorbed IPA molecule.

[a] Oxygen of OH of 2-propanol.

[b] Hydrogen of OH of 2-propanol.
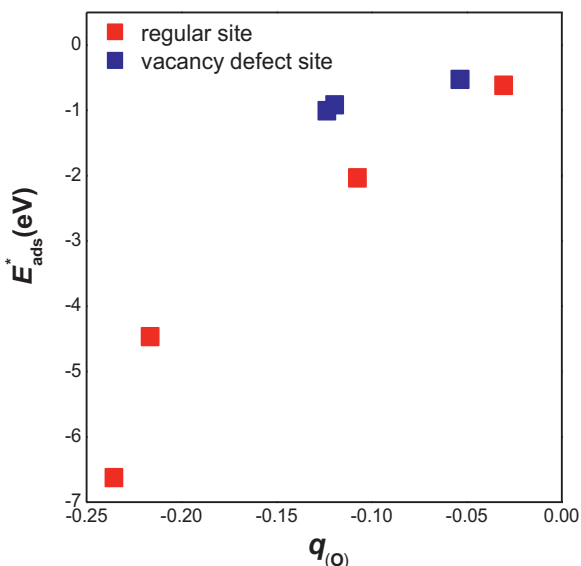
Fig. 7. Correlation between E^*_{ads} and the charge of O, $q(O)$, of adsorbed 2-propanol.

On F_s sites of terrace, edge and O-corner, the IPA adsorption is non-dissociative. The magnitude of E_{ads} for the F_s-edge and F_s-corner, i.e., those with lower coordination, are 0.4–0.5 eV larger in magnitude than that on F_s at terrace. On the other hand, the binding energy for terrace site is somewhat smaller, by about 0.1 eV, than that on the regular terrace. Whereas the $d_{(O-H)}$ and $d_{(C-O)}$ distances for the IPA molecule adsorbed on F_s-terrace are very similar to those on the regular terrace, the $d_{(O-Mg_s)}$ distance is about 0.7 Å shorter. On the other hand, these three distances for F_s-edge and F_s-corner are similar to those on Mg-corner. Notice that on all the F_s centers, an electrostatic interaction occurs between the H atom of IPA and the vacancy in which two electrons are trapped.

On V_s-corner, IPA adsorption is dissociative, with an E_{ads} whose magnitude is 1.6–1.8 eV higher than those corresponding to the other non-dissociative cases (O-edge and O-corner sites). In this geometry, the three oxygen atoms remaining after the elimination of the Mg atom at corner are highly reactive, giving a very distorted final geometry of IPA molecule, as revealed by the large value of the magnitude of E^*_{ads}. Notice also that the O atom of IPA is localized near the original position of the lacking Mg ion. The $d_{(H-O_s)}$ and $d_{(O-H)}$ distances in this geometry are similar to those found in dissociative adsorption on regular sites (O-edge and O-corner).

The analysis of atomic NBO charges for 2-propanol associative adsorption on vacancies of MgO (Table 4) reveals that they have the same tendency as in regular sites: the alcoholic O atom receives

negative charge whereas the magnitude of E^*_{ads} increases. This correlation can be appreciated looking at Fig. 7. An exception to this behavior is the V_s-corner site, where a depletion in the negative charge of the IPA oxygen atom is observed.

3.4. Evaluation of vibrational frequencies

The main calculated vibrational frequencies are summarized in Tables 2 and 3 for non-dissociative and dissociative adsorptions, respectively, together with the already presented experimental data.

The frequencies calculated for isolated 2-propanol were compared with the experimental data in gas phase [48,52]. We can identify all the assignments obtained experimentally. Most of the calculated frequency values present differences of about ±0.5%, but larger discrepancies are observed for $\nu(C-H_3)$, $\gamma(C-H)$ and $\delta(C-H)$, $\delta(O-H)$ vibration modes (0.9–2.3%).

Regarding the case of non-dissociative adsorption (i.e., terrace and Mg-corner for regular sites, and F_s-terrace, F_s-edge and F_s-corner) and comparing it with the frequencies for free IPA, we can notice several changes. As a result of the 2-propanol adsorption, the band corresponding to the O–H stretching suffers an important shift of ~520 to 630 cm^{-1} to lower frequencies. This is attributed to the enlargement of O–H bond (~0.03 to 0.04 Å) because a hydrogen bond is formed between the alcoholic H atom and a surface O_s anion, which weakened the O–H bond. On Mg-corner site, the shift of the band assigned to OH stretching is 235 cm^{-1} lower with respect to the value on terrace. In this case, this major shift to lower frequencies is the result not only of the hydrogen bond between the H atom of IPA and the surface oxygen, but also of the interaction between the Mg_{3c} cation and the alcoholic oxygen, which also contributes to weak the OH bond of IPA. On the other hand, the bands corresponding to $\gamma(C-H)$, $\nu(C-O)$, $\rho(C-H_3)$, and $\delta(C-H)$, $\delta(O-H)$ undergo a shift of ~22 to 80 cm^{-1} to higher frequencies, and the bands assigned to $\nu(C-H)$ present shifts of ~15 to 19 cm^{-1} to lower frequencies. These shifts are related to the small enlargement of the C–O bond (~0.01 to 0.02 Å) in the adsorbed 2-propanol molecule. In general, the bands assigned to $\nu(C-H_3)$, $\delta(C-H_3)$, $\nu(C-C)$, and $\rho(C-H_3)$ experience minor shifts (~9 cm^{-1}) from the structural modifications of the IPA adsorbed on the terrace surface.

In the case of dissociative adsorptions (i.e., on edge and O-corner topological defects, and on V_s-corner) the assignments corresponding to the formation of surface hydroxyl and isopropoxide species appear. Comparing the O–H bond at free alcohol with the one at edge and O-corner sites, a very large shift to lower values of frequencies are observed. The shift corresponding to the H–O_s bond stretching for defective edge is 1161 cm^{-1}, while that for the O-corner one is 335 cm^{-1}. These results are in agreement with the

distances of H—O_s and O—H bonds found in the optimized geometries. Indeed, the distances of H—O_s bond in these geometries are longer (1.03 Å for edge and 0.99 Å for O-corner) than the distance corresponding to O—H bond at free IPA (0.96 Å). The weakening of the O—H bond corresponding to the bond cleavage observed in these geometries is accompanied by the very close band due to adsorbed isopropoxide group. This is evidenced by the presence of a new band at about 2940 cm^{-1} assigned to $2\delta(C-H_3)_a$ and accompanied by the disappearance of the $\delta(C-H)$, $\delta(O-H)$ features. On the other hand, the bands assigned to $\nu(C-H_3)_a$, $\nu(C-H_3)_s$, $\delta(C-H_3)_a$, and $\delta(C-H_3)_s$ present higher shift than those observed on terrace, being these shifts for O-corner larger than those presented for edge site. The most important shift toward lower frequencies was presented for the band of C—H stretching, being these shifts of 104 cm^{-1} and 162 cm^{-1} for edge and O-corner, respectively. Besides, $\nu(C-O)$ and $\rho(C-H_3)$ present larger shifts ($\sim$60 cm^{-1}) than those observed for terrace.

Similarly to the geometries obtained on edge and O-corner, the adsorption of 2-propanol on V_s-corner is dissociative, as it can be observed if the corresponding bands are compared. The main modification corresponds to $\nu(O-H)$ band, which was assigned at 3719 cm^{-1}. In this case, this frequency corresponds to O_s—H bond between a surface oxygen anion surrounding the vacancy [37], and a H atom resulting from the IPA dissociative adsorption. Such as in the other dissociative geometries, the other assignments present the same tendency when they are compared with the frequencies observed on terrace.

4. Conclusions

The trends predicted by DFT calculations for the band shifts are in qualitative agreement with the ones observed from IR spectra. The differences between the experimental and theoretical frequencies were $\sim$10 to 60 cm^{-1}, although higher shifts were obtained for $\nu(O-H)$ band because MgO surface hydroxyls disturb this signal. The IPA evacuation of the catalytic cell showed that the bands corresponding to the isopropoxide species are in agreement with the bands theoretically obtained for edge and O-corner on regular sites and for V_s-corner, which indicates that IPA is dissociatively chemisorbed. The species corresponding to molecularly adsorbed IPA (predicted to occur on terrace and Mg-corner regular sites, and on F_s vacancies at terrace, edge and corner) were indirectly evaluated subtracting the spectrum resulting from the all adsorbed species from the spectrum corresponding to the chemisorbed species.

Combining the available experimental information and the theoretical results presented above, an important inference can be pointed out. From the experimental data for the 2-propanol adsorption on MgO, it is possible to conclude that this molecule dissociates easily. On the other hand, our theoretical calculations show that barrierless dissociation occurs only on edge and O-corner topological defects, and on the magnesium vacancy at Mg-corner (V_s sites). Therefore, the role of these sites could be predominant in the 2-propanol dehydrogenation [53], where the abstraction of a hydrogen atom from the alcohol is the first step in the reaction. In contrast, sites on regular terrace, Mg-corner sites and F_s sites on terrace, edge and corner, could be useful in reactions such as the hydrogenation of unsaturated ketones by hydrogen transfer reduction, where the non-dissociative adsorption of the alcohol is necessary in order to produce the transfer of a hydrogen atom of the alcoholic group (OH) to the unsaturated ketone [7].

References

[1] P. Mckendry, Bioresour. Technol. 83 (2002) 47–54.
[2] J.D. Adjaye, S.P.R. Katikaneni, N.N. Bakhshi, Fuel Process. Technol. 48 (1996) 115–143.
[3] A.G. Gayubo, A.T. Aguayo, A. Atutxa, R. Aguado, M. Olazar, J. Bilbao, Ind. Eng. Chem. Res. 43 (2004) 2619–2626.
[4] A.G. Gayubo, A.T. Aguayo, A. Atutxa, R. Aguado, J. Bilbao, Ind. Eng. Chem. Res. 43 (2004) 2610–2618.
[5] J.M. Campelo, A. Garcia, J.F. Herencia, D. Luna, J.M. Marinas, A.A. Romero, J. Catal. 151 (1995) 307–314.
[6] V.K. Díez, C.R. Apesteguía, J.I. Di Cosimo, Catal. Today 63 (2000) 53–62.
[7] J.J. Ramos, V.K. Díez, C.A. Ferretti, P.A. Torresi, C.R. Apesteguía, J.I. Di Cosimo, Catal. Today 172 (2011) 41–48.
[8] J.I. Di Cosimo, V.K. Diez, C.R. Apesteguia, Appl. Catal. 137 (1996) 149–166.
[9] H. Tsuji, H. Hattori, Catal. Today 116 (2006) 239–243.
[10] A. Corma, S. Iborra, J. Primo, F. Rey, Appl. Catal. 114 (1994) 215–225.
[11] C.A. Ferretti, S. Fuente, R. Ferullo, N. Castellani, C.R. Apesteguía, J.I. Di Cosimo, Appl. Catal. A: Gen. 413–414 (2012) 322–331.
[12] K. Tanabe, M. Misono, Y. Ono, H. Hattori, B. Delmom, J.T. Yates (Eds.), New Solid Acids and Bases. Their Catalytic Properties, Studies in Surface Science and Catalysis, vol. 51, Kodansha/Elsevier, Tokyo/Amsterdam, 1989.
[13] R.O. Kagel, R.G. Greenler, J. Chem. Phys. 49 (1968) 1638–1646.
[14] M.M. Branda, A.H. Rodríguez, P.G. Belelli, N.J. Castellani, Surf. Sci. 603 (2009) 1093–1098.
[15] M.M. Branda, R.M. Ferullo, P.G. Belelli, N.J. Castellani, Surf. Sci. 527 (2003) 89–99.
[16] C. Di Valentin, A. del Vitto, G. Pacchioni, S. Abbet, A.S. Wörz, K. Judai, U. Heiz, J. Phys. Chem. B 106 (2002) 11961–11969.
[17] M.M. Branda, P.G. Belelli, R.M. Ferullo, N.J. Castellani, Catal. Today 85 (2003) 153–165.
[18] C. Chizallet, G. Costentin, M. Che, F. Delbecq, P. Sautet, J. Phys. Chem. B 110 (2006) 15878–15886.
[19] A.D. Becke, J. Chem. Phys. 98 (1993) 5648–5652.
[20] R.M. Ferullo, S.A. Fuente, P.G. Belelli, N.J. Castellani, Surf. Sci. 603 (2009) 1262–1269.
[21] L. Giordano, J. Carrasco, C. Di Valentin, F. Illas, G. Pacchioni, J. Chem. Phys. 124 (2006) 174709.
[22] J. Carrasco, N. Lopez, F. Illas, H.-J. Freund, J. Chem. Phys. 125 (2006) 074711.
[23] J. Carrasco, C. Sousa, F. Illas, P.V. Sushko, A.L. Shluger, J. Chem. Phys. 125 (2006) 074710.
[24] S.F. Boys, F. Bernardi, Mol. Phys. 19 (1970) 553.
[25] W. Koch, M.C. Holthausen, A Chemist's Guide to Density Functional Theory, second ed., Wiley-VCH Verlag, 2001 (Chapter 12).
[26] A.E. Reed, L.A. Curtiss, F. Weinhold, Chem. Rev. 88 (1988) 899–926.
[27] A.P. Scout, L. Radom, J. Phys. Chem. 100 (1996) 16502.
[28] M.J. Frisch, et al., Gaussian 03, Revision C.02, Gaussian, Inc., Wallingford, CT, 2004.
[29] J.I. Di Cosimo, V.K. Díez, C. Ferretti, C.R. Apesteguía, Catalysis 26 (2014) 1–28.
[30] J.I. Di Cosimo, V.K. Díez, M. Xu, E. Iglesia, C.R. Apesteguía, J. Catal. 178 (1998) 499–510.
[31] R. Philipp, K. Fujimoto, J. Phys. Chem. 96 (1992) 9035–9038.
[32] C. Morterra, G. Ghiotti, F. Boccuzzi, S. Coluccia, J. Catal. 51 (1978) 299–313.
[33] M.I. Zaki, N. Sheppard, J. Catal. 80 (1983) 114–121.
[34] G.A.M. Hussein, N. Sheppard, M.I. Zaki, R.B. Fahim, J. Chem. Soc., Faraday Trans. 85 (1989) 1723–1742.
[35] M.I. Zaki, M.A. Hasan, L. Pasupulety, Langmuir 17 (2001) 4025–4033.
[36] G. Szollosi, M. Bartok, J. Mol. Catal. A: Chem. 148 (1999) 265–273.
[37] C. Chizallet, G. Costentin, M. Che, F. Delbocq, P. Sautet, J. Am. Chem. Soc. 129 (2007) 6442–6451.
[38] M.I. Zaki, M.A. Hasan, L. Pasupulety, Langmuir 17 (2001) 4025–4035.
[39] H. Miyata, M. Wakamiya, Y. Kubokawa, J. Catal. 34 (1974) 117–126.
[40] H. Madhavaram, H. Idriss, J. Catal. 206 (2002) 155–163.
[41] G. Szöllösi, M. Bartók, J. Mol. Struct. 482–483 (1999) 13–17.
[42] J. Gallas, C. Binet, Adv. Mol. Relax. Interact. Process. 24 (1982) 191–198.
[43] F. Kooli, C. Martín, V. Rives, Langmuir 13 (1997) 2303–2312.
[44] P. Rossi, G. Busca, V. Lorenzelli, O. Saur, J. Lavalley, Langmuir 3 (1987) 52–60.
[45] D. Treibmann, A. Simon, Ber. Bunsenges. Phys. Chem. 70 (1966) 562–571.
[46] R.K. Grasselli, J.D. Burrington, Adv. Catal. 30 (1981) 133–142.
[47] H. Madhavaram, H. Idriss, Stud. Surf. Sci. Catal. 110 (1997) 265–274.
[48] R. King, H. Idriss, Langmuir 25 (2009) 4543–4552.
[49] M.S. Snow, B.J. Howard, L. Evangelisti, W. Caminati, J. Phys. Chem. A 115 (2011) 47–56.
[50] E. Hirota, Y. Kawashima, J. Mol. Spectrosc. 207 (2001) 243–252.
[51] A.F. Wells, Structural Inorganic Chemistry, fifth ed., Clarendon Press, Oxford, 1984, pp. 1004–1012.
[52] H. Madhavaram, H. Idriss, J. Catal. 206 (2002) 155–164.
[53] F. Braum, J.I. Di Cosimo, Catal. Today 116 (2006) 206–215.